Inelastic x-ray scattering as a probe of electronic correlations

T. P. Devereaux and G. E. D. McCormack
Department of Physics, University of Waterloo, Waterloo, Ontario, Canada N2L 3G1

J. K. Freericks
Department of Physics, Georgetown University, Washington, DC 20057, USA
(Received 7 May 2003; published 8 August 2003)

We construct an exact dynamical mean-field theory for nonresonant inelastic light scattering in the infinite-dimensional Falicov-Kimball model, which can be tuned through a quantum critical metal-insulator transition. Due to the projection of the polarization orientations onto different regions of the Brillouin zone and due to the transfer of energy and momentum from the weakly to the strongly correlated charge excitations, the nature of the dynamics can be naturally interpreted as strongly temperature-dependent low-energy particle-hole excitations and weakly temperature-dependent high-energy charge-transfer excitations which depend delicately on the electronic correlations. These results can be used to provide important information concerning the evolution of charge dynamics in different regions of the Brillouin zone.

DOI: 10.1103/PhysRevB.68.075105 PACS number(s): 78.70.Ck, 72.80.Sk, 78.66.Nk, 71.30.+h

I. INTRODUCTION

Inelastic x-ray scattering (with meV accuracy over a spectral range of several eV's) has improved significantly over the past few years due to the increased photon flux of third-generation synchrotron sources.[1–11] The large cross section of light-coupled probes (as compared to neutron scattering, for example) allows for a systematic study of the dispersive charge dynamics in a wide dynamical range $(\mathbf{q},\Omega)$ in solids and fluids. It has opened an additional window to study correlation effects on phonons,[2] plasmons,[3] quasiparticles,[4] charge-transfer excitations,[5–10] and orbital excitations.[11] One particular point of interest has been the study of the evolution of strongly correlated systems as some parameter of the system, such as the electron density, is varied by doping or pressure. While many single-particle properties have been studied via angle-resolved photoemission, important questions concerning the evolution of the unoccupied states are now directly accessible via inelastic x-ray scattering.

Recent experiments have focused on a number of correlated (Mott) insulators such as La_2CuO_4 and $Sr_2CuO_2Cl_2$,[6] $Ca_2CuO_2Cl_2$,[7] NaV_2O_5,[8] Nd_2CuO_4,[9] and one-dimensional insulators Sr_2CuO_3 and Sr_2CuO_2.[10] The measurements have revealed dispersive high-energy and low-energy excitations which have been identified with a photon-induced charge transfer between different atomic orbitals or with transitions from the lower to the upper Hubbard band across an effective **q**-dependent Mott gap.

More recent measurements have begun to appear in materials doped from their parent Mott insulating phases.[12] However, the theoretical development of inelastic x-ray scattering in strongly correlated metals and insulators is just beginning.[13–17] Of particular interest is a determination of how the upper and lower Hubbard bands, and consequently, the Mott gap evolve with correlations. As experiments reach higher and higher resolution, it will shortly be possible to track the evolution of electronic correlations from strongly correlated insulators to strongly and then weakly correlated metals. The purpose of this contribution is to investigate such a theory for inelastic x-ray scattering. In particular, we develop an exact dynamical mean-field theory for nonresonant inelastic light scattering in a system which can be tuned across the quantum critical point of a metal-insulator transition. We calculate the inelastic x-ray cross section on both sides of the transition and near the critical point.

The outline of this paper is as follows. In Sec. II we develop the general formalism for nonresonant inelastic x-ray scattering and review simple physical ideas for weakly correlated metals. In Sec. III, we present the specific formalism for calculating the x-ray response in the Falicov-Kimball model in the limit of large spatial dimensions and in Sec. IV we present the numerical results. Finally, we summarize our results and discuss them in light of the recent measurements in Sec. V. This paper expands the results for the insulating phase[14] to consider metals and materials close to the metal-insulator transition.

II. FORMALISM

A. Nonresonant response

Light can scatter off of many different excitations in a system, but here we focus on the inelastic scattering of x rays from electrons. X rays, unlike optical photons, can exchange both energy and momentum when they scatter with a solid. The scattering occurs as light creates charge fluctuations in different locations of the Brillouin zone (BZ). These charge fluctuations are classified as either isotropic charge fluctuations or anisotropic charge fluctuations (which vanish when averaging their **k**-space variation over the BZ). The way in which the charge fluctuations are created is dictated by the polarization orientation of the incoming and outgoing photons set by the scattering geometry. These polarization orientations transform according to the operations of the point-group symmetry of the crystal, and so must the charge fluctuations that they create. It is through this mechanism that the charge excitations in different regions of the BZ can be systematically selected and explored via inelastic light scattering.

These charge fluctuations relax by internal scattering processes, such as due to impurities or Coulomb scattering, and finally via the reemission of photons; inelastic x-ray scattering probes these relaxation processes at different regions of the BZ and at different transferred energies. An important distinction between isotropic and anisotropic charge fluctuations is that the former are coupled to long-range Coulomb interactions, while the latter are not. This has significant consequences on the polarization dependence of the observed spectra. We now elaborate upon this further.

We limit our focus to the case of nonresonant x-ray scattering, since resonant processes have not yet been treated exactly in any correlated itinerant model. The inelastic x-ray response is given formally by a generalized density-density correlation function $S(\mathbf{q},\omega)=-(1/\pi)[1+n(\omega)]\chi''(\mathbf{q},\omega)$, with

$$\chi(\mathbf{q},\omega)=\langle[\tilde{\rho}(\mathbf{q}),\tilde{\rho}(-\mathbf{q})]\rangle_{(\omega)}, \tag{1}$$

formed with an ''effective'' density operator given by

$$\tilde{\rho}(\mathbf{q})=\sum_{\mathbf{k},\sigma}\gamma_a(\mathbf{k})c^{\dagger}_{\sigma}(\mathbf{k}+\mathbf{q}/2)c_{\sigma}(\mathbf{k}-\mathbf{q}/2), \tag{2}$$

$n(\omega)$ denoting the Bose distribution function, and the double prime superscript denoting the imaginary part. We relate the inelastic light-scattering vertex γ_a to the curvature of the energy band $\epsilon(\mathbf{k})=-t^*\Sigma_{j=1}^{\infty}\cos\mathbf{k}_j/\sqrt{d}$ and the light polarizations through

$$\gamma_a(\mathbf{k})=\sum_{\alpha,\beta}e^s_{\alpha}\frac{\partial^2\epsilon(\mathbf{k})}{\partial k_{\alpha}\partial k_{\beta}}e^i_{\beta}. \tag{3}$$

This holds in the limit of vanishing energy transfers, but can also be generalized in terms of Brillouin-zone harmonics to other nonresonant cases. Here, $\mathbf{e}^{i,s}$ denote the incident and scattered x-ray polarization vectors, respectively, and we choose units $k_B=c=\hbar=1$ and set the lattice constant equal to 1. We can classify the scattering amplitudes by their point-group symmetry operations. It is customary to have A_{1g} denote the symmetry of the lattice (s wave) and B_{1g} and B_{2g} denote two of the d wave symmetries. For any dimension $d>1$, if we choose $e^i=(1,1,1,\ldots)$ and $e^s=(1,-1,-1,\ldots)$, then we have the B_{1g} sector, while $e^i=e^s=(1,1,1,\ldots)$ projects out the A_{1g} sector, since the B_{2g} component is identically zero for models with only nearest-neighbor hopping. Thus, we can cast the scattering amplitudes into a simple form: $\gamma_{A_{1g}}(\mathbf{k})=-\epsilon(\mathbf{k})$ and $\gamma_{B_{1g}}(\mathbf{k})=t^*\Sigma_{j=1}^{\infty}\cos\mathbf{k}_j(-1)^j/\sqrt{d}$, which recovers the $d=2$ representations of the tetragonal point-group symmetry operations commonly used in CuO_2 systems. We note that if we take the pure charge vertex for A_{1g}, $\gamma_{A_{1g}}=1$, then $S(q,\omega)\propto\mathrm{Im}\{1/\epsilon(\mathbf{q},\omega)\}$, with ϵ the dielectric function.[18]

B. Weakly correlated electrons

It is useful to review the nonresonant response for weakly correlated metals to determine where we expect to see the role of correlations emerge. For noninteracting electrons the effective density response is given in terms of a generalized Lindhard function which incorporates the symmetry dependence of the light-scattering amplitudes γ in the Lindhard kernel.[19] In particular, in the limit $\mathbf{q}\to 0$ there is no low-energy inelastic light scattering (for three dimensions) as there is no phase space to create electron-hole pairs, and the only excitation is the high-energy collective plasmon. This is analogous to the situation of the charge susceptibility, which vanishes at finite frequencies when $\mathbf{q}=0$ because the total charge of the system commutes with the Hamiltonian. For finite $\mathbf{q}$, the particle-hole continuum gives low-energy scattering up to a frequency of v_Fq (with v_F the Fermi velocity). When scattering off an impurity potential $V_{\mathbf{k},\mathbf{k}'}$ is added this sharp cutoff is smeared, and scattering occurs over a wide range of transferred frequencies. The density response at small $\mathbf{q}$ is given by an effective density-density Kubo formula[19]

$$\chi''_{LL}(\mathbf{q},\Omega)=N_F\frac{\Omega\tilde{\tau}_L^{-1}}{\Omega^2+\tilde{\tau}_L^{-2}}, \tag{4}$$

with N_F the density of states at the Fermi level and τ_L^{-1} the relaxation rate for density fluctuations having a symmetry selected by light orientations labeled by L (L denotes an irreducible representation of the point group of the crystal, such as A_{1g} or B_{1g} for a tetragonal crystal; we use $L=0$ to denote the A_{1g} sector). Expanding the impurity potential in terms of a complete set of basis functions $\phi_L(\mathbf{k})$ yields

$$|V_{\mathbf{k},\mathbf{k}'}|^2=\sum_L\phi^*_L(\mathbf{k}')\Gamma_L\phi_L(\mathbf{k}). \tag{5}$$

The width and location of the peak of the response is given by $\tilde{\tau}_L^{-1}=\tau_{L=0}^{-1}-\tau_L^{-1}+Dq^2$, where $\tau_L^{-1}=2\pi N_F\Gamma_L$ is the scattering rate that preserves charge fluctuations having symmetry L and D is the diffusion constant related to the resistivity ρ by an Einstein relation $D^{-1}=2e^2N_F\rho$. Here, we have assumed that the impurity potential is rotationally invariant and largely independent of momentum transfer. Thus in this case, phase space is already created by the impurity scattering potential for anisotropic ($L\neq 0$) density fluctuations coupled to the x rays. However, isotropic density fluctuations ($L=0$) are governed by the continuity equation and must vanish at $\mathbf{q}=0$ even in the presence of an impurity potential. Therefore, for $L\neq 0$ channels (B_{1g}) the x-ray response has a Lorenzian line shape with a peak position and width which grows as q^2 for momentum transfers away from the zone center $q=0$, while for $L=0$ (A_{1g}), there is only low-energy scattering for finite q due to particle-number conservation.

III. FORMALISM WITH CORRELATIONS

Coulomb interactions create phase space for particle-hole excitations and lead to inelastic scattering even at $\mathbf{q}=0$ for channels not having the underlying symmetry of the lattice. The scattering can be enhanced when the momentum structure of the Coulomb interaction is considered further. For example, in a material having a nested or slightly nested Fermi surface (FS) at some points in the BZ, the resulting

response would be enhanced for polarization orientations which highlight the nested or nearly nested regions of the FS.[20] In the case of antiferromagnetic interactions which are strong for momentum transfers of (π,π), the response is appreciably modified for the B_{1g} channel in two-dimensional tetragonal systems.[21] The dispersion of these excitations can then be tracked as a function of light momentum transfers $\mathbf{q}$ just as they can via neutron scattering. Thus, in principle, inelastic x-ray scattering systematically tracks the role of correlations and the accompanying FS instabilities by exploring the polarization dependence and momentum-transfer dependence of the resulting spectra.

In this paper, we are interested in carrying out calculations in which electronic correlations can be handled exactly in a system which can be tuned through a quantum critical point. The Falicov-Kimball model, which has been used to describe a variety of phenomenon in binary alloys, rare-earth compounds, and intermediate-valence materials,[22] contains itinerant band electrons and localized electrons, in which the band electrons can hop with amplitude[23] $t^*/2\sqrt{d}$ between nearest neighbors on a d-dimensional hypercubic lattice and interact via a screened Coulomb interaction U with the localized electrons:

$$H=-\frac{t^*}{2\sqrt{d}}\sum_{\langle i,j\rangle} c_i^\dagger c_j+E_f\sum_i w_i-\mu\sum_i c_i^\dagger c_i+U\sum_i c_i^\dagger c_i w_i, \tag{6}$$

where $c_i^\dagger, c_i$ is the spinless conduction-electron creation (annihilation) operator at site i and $w_i=0$ or 1 is a classical variable for the localized electron number at site i. E_f and μ control the filling of the localized and conduction electrons, respectively. We restrict consideration to half filling $\langle c_i^\dagger c_i\rangle=\langle w_i\rangle=1/2$.

In this model, at half-filling, the system possesses[24] a non-Fermi-liquid metallic ground state for $U<U_c$ and an insulating state for $U>U_c$. The single-particle density of states (DOS) at the Fermi level (FL) vanishes at the critical $U_c\approx 1.5t^*$ and the self-energy develops a pole. As U approaches U_c from below, a pseudogap develops near the FL and for $U>U_c$ the DOS evolves into lower and upper Hubbard bands separated at the band centers by U. However, the DOS is independent of temperature (aside from a trivial shift due to the temperature dependence of the chemical potential, if applicable) and thus it is not possible to determine the particle dynamics from the single-particle properties alone.[24]

The many-body problem is solved[25] by first recognizing that the self-energy and relevant irreducible vertex functions are local and then mapping the local objects of the lattice problem onto an effective atomic problem in a time-dependent dynamical field λ. In this procedure, we are interested in calculating the local Green's function, which is defined by

$$G(\tau)=-\mathrm{Tr}_{cf}\mathcal{T}_\tau\langle e^{-\beta H}c(\tau)c^\dagger(0)S(\lambda)\rangle/Z(\lambda) \tag{7}$$

for imaginary times τ. Here, Tr_{cf} denotes the trace over conduction and localized electrons and $\mathcal{T}_\tau$ denotes the time-ordering operator. The partition function is $Z(\lambda)=\mathrm{Tr}_{cf}\mathcal{T}_\tau\langle\exp[-\beta H]S(\lambda)\rangle$, with the evolution operator S defined by

$$S(\lambda)=\exp\left[-\int_0^\beta d\tau\int_0^\beta d\tau' c^\dagger(\tau)\lambda(\tau,\tau')c(\tau')\right]. \tag{8}$$

In these equations the Hamiltonian is the atomic Hamiltonian, which has $t^*=0$ and all time dependence is with respect to this atomic Hamiltonian.

In order to determine the Green's function anywhere in the complex plane, we follow the iterative algorithm of Jarrell:[26] (i) begin with the self-energy Σ set equal to zero; (ii) determine the local lattice Green's function from the Hilbert transform,

$$G(z)=\int d\epsilon\rho(\epsilon)\frac{1}{z+\mu-\Sigma(z)-\epsilon}, \tag{9}$$

with $\rho(\epsilon)$ the noninteracting DOS (a Gaussian here); (iii) extract the effective medium G_0 from $G^{-1}(z)+\Sigma(z)=G_0^{-1}(z)$; (iv) calculate the new Green's function from $G(z)=(1-w_1)G_0(z)+w_1/[G_0^{-1}(z)-U]$; and (v) extract the new self-energy from $\Sigma(z)=G_0^{-1}(z)-G^{-1}(z)$. Steps (ii) through (v) are repeated until the iterations converge. Sometimes we need to perform weighted averages of the iterations to attain convergence. We usually work with solutions that are converged to at least one part in 10^8. Using this algorithm, we can determine the Green's function and self-energy either along the imaginary axis or along the real axis. These solutions are then employed to calculate the inelastic light-scattering response functions.

The inelastic light scattering is calculated by evaluating the density-density correlation function defined in Eq. (1). The Bethe-Salpeter equation for the susceptibility is shown schematically in Fig. 1. Note that there are two coupled equations, which differ by the number of factors of the inelastic light-scattering vertex that are present. The solid lines denote dressed Green's functions in momentum space, and the symbol Γ denotes the local irreducible charge vertex. The calculation of the relevant momentum summations implied in Fig. 1 is nontrivial. The starting point is the determination of the direction in momentum space in which the transferred momentum $\mathbf{q}$ lies. In this contribution we consider two different directions: (i) the zone diagonal, where $\mathbf{q}=(q,q,q,\ldots,q)$ and (ii) a generalized "zone boundary," where $\mathbf{q}=(0,q,0,q,0,q,\ldots,0,q)$ or $\mathbf{q}=(q,\pi,q,\pi,q,\pi,\ldots,q,\pi)$; in all cases we vary $0\leqslant q\leqslant\pi$. We choose to call the wave vector in (ii) the zone boundary because it reduces to the two-dimensional zone boundary when $d=2$ and it is a nontrivial generalization in the infinite-dimensional limit. If, on the other hand, we examine the true infinite-dimensional zone boundary, where only one dimension has a nonzero wave vector component, then that zone boundary maps onto the zone-center wave vector (since only one of the d-components is nonzero), and there is no dispersion. From now on we will refer to the generalized zone-boundary direction as the zone-boundary direction.

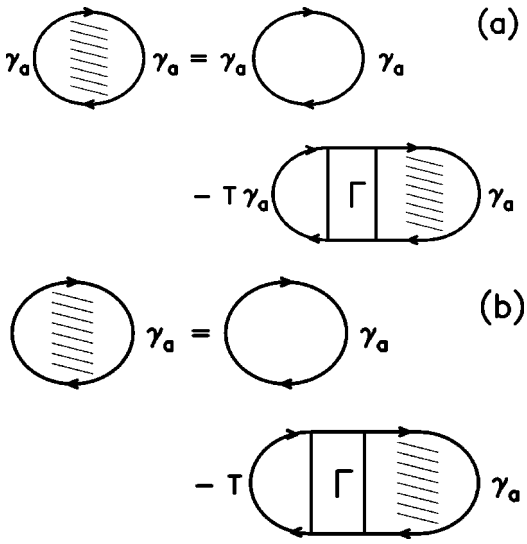

FIG. 1. Coupled Dyson equations for the inelastic light-scattering density-density correlation functions described by the scattering amplitude γ_a. Panel (a) depicts the Dyson equation for the interacting correlation function, while panel (b) is the supplemental equation needed to solve for the correlation function (the difference in the two equations is the number of γ_a factors). The symbol Γ stands for the local dynamical irreducible charge vertex. In situations where there are no charge vertex corrections (such as B_{1g} scattering along the zone diagonal), the correlation function is simply given by the first (bare-bubble) diagram on the right-hand side of panel (a).

When evaluating the density-density correlation function, we will need to evaluate momentum summations of the form[27]

$$\sum_{\mathbf{k}} \sum_{j} \cos\left(k_j + \frac{q_j}{2}\right) \frac{1}{z+\mu-\Sigma(z)-\epsilon(\mathbf{k})} \times \frac{1}{z+\mu-\Sigma(z)-\epsilon(\mathbf{k}+\mathbf{q})} \tag{10}$$

for the A_{1g} sector and

$$\sum_{\mathbf{k}} \sum_{j} \cos\left(k_j + \frac{q_j}{2}\right)(-1)^j \frac{1}{z+\mu-\Sigma(z)-\epsilon(\mathbf{k})} \times \frac{1}{z+\mu-\Sigma(z)-\epsilon(\mathbf{k}+\mathbf{q})} \tag{11}$$

for the B_{1g} sector. In the above equations, z denotes a number in the complex plane. The summation can be evaluated by first rewriting each momentum-dependent Green's function as an integral of an exponential function

$$\frac{1}{z+\mu-\Sigma(z)-\epsilon(\mathbf{k})} = -i\int_0^\infty d\lambda\, e^{i\lambda[z+\mu-\Sigma(z)-\epsilon(\mathbf{k})]}, \tag{12}$$

and then expanding each band-structure energy in terms of the summation over each component of the wave vector. Then the integral over momentum factorizes into an infinite product of one-dimensional integrals. Each integral needs to be expanded just to the order of $1/d$, and the resulting terms can be exponentiated into a form that has a Gaussian dependence on λ. The Gaussian integral can then be evaluated directly. When we do this, we find that the relevant bare susceptibilities have all of their $\mathbf{q}$ dependence summarized in the form of two scalar parameters

$$X = \lim_{d\to\infty} \frac{1}{d} \sum_{j=1}^{d} \cos q_j \tag{13}$$

and

$$X'_{A_{1g}} = \lim_{d\to\infty} \frac{1}{d} \sum_{j=1}^{d} \cos\frac{q_j}{2}, \qquad X'_{B_{1g}} = \lim_{d\to\infty} \frac{1}{d} \sum_{j=1}^{d} (-1)^j \cos\frac{q_j}{2}. \tag{14}$$

In situations where the summation in Eqs. (11) or (12) vanish, the response function is not renormalized by the irreducible charge vertex, and it can be expressed solely in terms of the bare response function (this phenomenon was first seen for the optical conductivity[28]). This never occurs for the A_{1g} channel, but it does occur for the B_{1g} channel when $\mathbf{q}$ lies on the zone diagonal. In all other cases, the response function is renormalized by the irreducible charge vertex,[29] which takes the form

$$\Gamma(i\omega_m, i\omega_n; i\nu_{l\neq 0}) = \delta_{mn} \frac{1}{T} \frac{\Sigma_m - \Sigma_{m+l}}{G_m - G_{m+l}} \tag{15}$$

on the imaginary axis [$i\omega_m = i\pi T(2m+1)$ is the fermionic Matsubara frequency and $i\nu_l = 2i\pi Tl$ is the bosonic Matsubara frequency]. Here, $\Sigma_m = \Sigma(i\omega_m)$ is the local self-energy on the imaginary axis and $G_m = G(i\omega_m)$ is the local Green's function on the imaginary axis. These vertex corrections are particularly crucial for the A_{1g} symmetry in order to satisfy Ward identities and particle-number conservation. Note that the vertex corrections enter for the different symmetry channels away from the zone diagonal because at a finite momentum transfer, the different symmetry representations generically mix together.

The strategy for determining the final forms for the response functions on the real axis is to first calculate the response functions on the imaginary axis and then replace Matsubara frequency summations by contour integrals that surround the poles of the Fermi-Dirac distribution function $f(\omega) = 1/[1+\exp(\beta\omega)]$ with $\beta = 1/T$. Then, the contours are deformed to be parallel to the real axis, and terms that depend on the bosonic Matsubara frequency as $f(\omega + i\nu_l)$ are replaced by $f(\omega)$. Finally, we analytically continue the bosonic Matsubara frequencies from the imaginary to the real axis. This procedure was carried out in detail for the Raman response[30] and will not be repeated here.

The final formulas for the response functions are complicated integrals of functions that depend on one of the six different bare susceptibilities. These six bare susceptibilities are

$$\chi_0(\omega;X,\nu)=-\int_{-\infty}^{\infty}d\epsilon\rho(\epsilon)\frac{1}{\omega+\mu-\Sigma(\omega)-\epsilon}\frac{1}{\sqrt{1-X^2}}F_\infty\left(\frac{\omega+\nu+\mu-\Sigma(\omega+\nu)-X\epsilon}{\sqrt{1-X^2}}\right), \tag{16}$$

$$\tilde{\chi}_0(\omega;X,\nu)=-\int_{-\infty}^{\infty}d\epsilon\rho(\epsilon)\frac{1}{\omega+\mu-\Sigma^*(\omega)-\epsilon}\frac{1}{\sqrt{1-X^2}}F_\infty\left(\frac{\omega+\nu+\mu-\Sigma(\omega+\nu)-X\epsilon}{\sqrt{1-X^2}}\right), \tag{17}$$

$$\chi_0'(\omega;X,\nu)=\frac{X'}{2}\int_{-\infty}^{\infty}d\epsilon\rho(\epsilon)\left\{\frac{\frac{1}{\sqrt{1-X^2}}F_\infty\left(\frac{\omega+\nu+\mu-\Sigma(\omega+\nu)-X\epsilon}{\sqrt{1-X^2}}\right)}{[\omega+\mu-\Sigma(\omega)-\epsilon]^2}\right.$$
$$\left.-\frac{2}{1-X^2}\frac{1-\frac{\omega+\nu+\mu-\Sigma(\omega+\nu)-X\epsilon}{\sqrt{1-X^2}}F_\infty\left(\frac{\omega+\nu+\mu-\Sigma(\omega+\nu)-X\epsilon}{\sqrt{1-X^2}}\right)}{\omega+\mu-\Sigma(\omega)-\epsilon}\right\}, \tag{18}$$

$$\tilde{\chi}_0'(\omega;X,\nu)=\frac{X'}{2}\int_{-\infty}^{\infty}d\epsilon\rho(\epsilon)\left\{\frac{\frac{1}{\sqrt{1-X^2}}F_\infty\left(\frac{\omega+\nu+\mu-\Sigma(\omega+\nu)-X\epsilon}{\sqrt{1-X^2}}\right)}{[\omega+\mu-\Sigma^*(\omega)-\epsilon]^2}\right.$$
$$\left.-\frac{2}{1-X^2}\frac{1-\frac{\omega+\nu+\mu-\Sigma(\omega+\nu)-X\epsilon}{\sqrt{1-X^2}}F_\infty\left(\frac{\omega+\nu+\mu-\Sigma(\omega+\nu)-X\epsilon}{\sqrt{1-X^2}}\right)}{\omega+\mu-\Sigma^*(\omega)-\epsilon}\right\}, \tag{19}$$

$$\bar{\chi}_0(\omega;X,\nu)=\frac{\chi_0(\omega;X,\nu)}{2}-\frac{X'^2}{2}\int_{-\infty}^{\infty}d\epsilon\rho(\epsilon)\left\{\frac{\frac{1}{\sqrt{1-X^2}}F_\infty\left(\frac{\omega+\nu+\mu-\Sigma(\omega+\nu)-X\epsilon}{\sqrt{1-X^2}}\right)}{[\omega+\mu-\Sigma(\omega)-\epsilon]^3}-\frac{2}{1-X^2}\frac{1-\frac{\omega+\nu+\mu-\Sigma(\omega+\nu)-X\epsilon}{\sqrt{1-X^2}}F_\infty\left(\frac{\omega+\nu+\mu-\Sigma(\omega+\nu)-X\epsilon}{\sqrt{1-X^2}}\right)}{[\omega+\mu-\Sigma(\omega)-\epsilon]^2}\right.$$
$$\left.-\frac{1}{(1-X^2)^{3/2}}\frac{\left\{F_\infty\left(\frac{\omega+\nu+\mu-\Sigma(\omega+\nu)-X\epsilon}{\sqrt{1-X^2}}\right)+2\frac{\omega+\nu+\mu-\Sigma(\omega+\nu)-X\epsilon}{\sqrt{1-X^2}}\left[1-\frac{\omega+\nu+\mu-\Sigma(\omega+\nu)-X\epsilon}{\sqrt{1-X^2}}F_\infty\left(\frac{\omega+\nu+\mu-\Sigma(\omega+\nu)-X\epsilon}{\sqrt{1-X^2}}\right)\right]\right\}}{\omega+\mu-\Sigma(\omega)-\epsilon}\right\}, \tag{20}$$

and

$$\bar{\tilde{\chi}}_0(\omega;X,\nu)=\frac{\tilde{\chi}_0(\omega;X,\nu)}{2}-\frac{X'^2}{2}\int_{-\infty}^{\infty}d\epsilon\rho(\epsilon)\left\{\frac{\frac{1}{\sqrt{1-X^2}}F_\infty\left(\frac{\omega+\nu+\mu-\Sigma(\omega+\nu)-X\epsilon}{\sqrt{1-X^2}}\right)}{[\omega+\mu-\Sigma^*(\omega)-\epsilon]^3}-\frac{2}{1-X^2}\frac{1-\frac{\omega+\nu+\mu-\Sigma(\omega+\nu)-X\epsilon}{\sqrt{1-X^2}}F_\infty\left(\frac{\omega+\nu+\mu-\Sigma(\omega+\nu)-X\epsilon}{\sqrt{1-X^2}}\right)}{[\omega+\mu-\Sigma^*(\omega)-\epsilon]^2}-\frac{1}{(1-X^2)^{3/2}}\right.$$
$$\left.\times\frac{\left\{F_\infty\left(\frac{\omega+\nu+\mu-\Sigma(\omega+\nu)-X\epsilon}{\sqrt{1-X^2}}\right)+2\frac{\omega+\nu+\mu-\Sigma(\omega+\nu)-X\epsilon}{\sqrt{1-X^2}}\left[1-\frac{\omega+\nu+\mu-\Sigma(\omega+\nu)-X\epsilon}{\sqrt{1-X^2}}F_\infty\left(\frac{\omega+\nu+\mu-\Sigma(\omega+\nu)-X\epsilon}{\sqrt{1-X^2}}\right)\right]\right\}}{\omega+\mu-\Sigma^*(\omega)-\epsilon}\right\}. \tag{21}$$

In these equations, $F_\infty(z)=\int d\epsilon\rho(\epsilon)/(z-\epsilon)$ is the Hilbert transform of the noninteracting DOS [$\rho(\epsilon)=\exp(-\epsilon^2)/\sqrt{\pi}$].

The A_{1g} and B_{1g} responses both can be written as

$$\chi(\mathbf{q},\nu)=\frac{i}{2\pi}\int_{-\infty}^{\infty}d\omega\Bigg\{ f(\omega)\frac{\overline{\chi}_0(\omega;X,\nu)+\frac{\Sigma(\omega)-\Sigma(\omega+\nu)}{G(\omega)-G(\omega+\nu)}[\chi_0(\omega;X,\nu)\overline{\chi}_0(\omega;X,\nu)-\chi_0'^2(\omega;X,\nu)]}{1+\frac{\Sigma(\omega)-\Sigma(\omega+\nu)}{G(\omega)-G(\omega+\nu)}\chi_0(\omega;X,\nu)}$$

$$-f(\omega+\nu)\frac{\overline{\chi}_0^*(\omega;X,\nu)+\frac{\Sigma^*(\omega)-\Sigma^*(\omega+\nu)}{G^*(\omega)-G^*(\omega+\nu)}[\chi_0^*(\omega;X,\nu)\overline{\chi}_0^*(\omega;X,\nu)-\chi_0'^{2*}(\omega;X,\nu)]}{1+\frac{\Sigma^*(\omega)-\Sigma^*(\omega+\nu)}{G^*(\omega)-G^*(\omega+\nu)}\chi_0^*(\omega;X,\nu)}$$

$$-[f(\omega)-f(\omega+\nu)]\frac{\tilde{\overline{\chi}}_0(\omega;X,\nu)+\frac{\Sigma^*(\omega)-\Sigma(\omega+\nu)}{G^*(\omega)-G(\omega+\nu)}[\tilde{\chi}_0(\omega;X,\nu)\tilde{\overline{\chi}}_0(\omega;X,\nu)-\tilde{\chi}_0'^2(\omega;X,\nu)]}{1+\frac{\Sigma^*(\omega)-\Sigma(\omega+\nu)}{G^*(\omega)-G(\omega+\nu)}\tilde{\chi}_0(\omega;X,\nu)}\Bigg\}, \tag{22}$$

In the case of the A_{1g} response on the zone diagonal $\mathbf{q}=(q,q,\ldots,q)$, we have $X=\cos q$ and $X'=\cos q/2=\sqrt{(1+X)/2}$. In the case of the A_{1g} response on the zone edge, we have $X=(1+\cos q)/2$ and $X'=(1+\cos q/2)/2=(1+\sqrt{X})/2$ for $\mathbf{q}=(0,q,0,q,\ldots,0,q)$ and $X=(\cos q-1)/2$ and $X'=\cos(q/2)/2=\sqrt{(1+X)/2}$ for $\mathbf{q}=(q,\pi,q,\pi,\ldots,q,\pi)$. In the case of the B_{1g} response on the zone edge, we have $X=(1+\cos q)/2$ and $X'=(-1+\cos q/2)/2=(-1+\sqrt{X})/2$ for $\mathbf{q}=(0,q,0,q,\ldots,0,q)$ and $X=(\cos q-1)/2$ and $X'=-\cos(q/2)/2=-\sqrt{(1+X)/2}$ for $\mathbf{q}=(q,\pi,q,\pi,\ldots,q,\pi)$. The case of the B_{1g} response on the zone diagonal is much simpler, because it does not have any renormalizations due to the charge vertex and does not depend on X'. It becomes

$$\chi_{B_{1g}}(\mathbf{q},\nu)=\frac{i}{4\pi}\int_{-\infty}^{\infty}d\omega\{f(\omega)\chi_0(\omega;X,\nu)$$
$$-f(\omega+\nu)\chi_0^*(\omega;X,\nu)$$
$$-[f(\omega)-f(\omega+\nu)]\tilde{\chi}_0(\omega;X,\nu)\}. \tag{23}$$

There is a special point in momentum space, where the response functions become simple again. This occurs at the $(\pi,\pi,\ldots,\pi)$ point, where $X=-1$ and $X'=0$. In this case, $\chi_0'=0$ and $\overline{\chi}_0$ is proportional to χ_0, so the Bethe-Salpeter equation factorizes, and the susceptibility in Eq. (22) becomes proportional to the bare susceptibility *for any symmetry*. Hence, the A_{1g} response and the B_{1g} response are identical at that point in the BZ. In fact, this result implies that polarized measurements at the zone-corner point can immediately show the effects of nonlocal charge fluctuations on the inelastic x-ray response functions, since any deviation of the A_{1g} signal from the B_{1g} signal arises from effects of nonlocal charge fluctuations. *We feel this may be one of the cleanest experimental tests for the importance of nonlocal charge fluctuations in a correlated many-body system.*

Finally, a careful examination of Eqs. (16)–(22) shows that the response function depends only on X'^2. Since the only difference for the A_{1g} and B_{1g} responses along the zone edge (for $-1\leqslant X\leqslant 0$) is a sign change in X', the x-ray scattering is identical for the A_{1g} and B_{1g} channels along the zone edge for $-1\leqslant X\leqslant 0$. It might be difficult to locate the relevant path in the BZ that would show this behavior in two or three dimensions, so examining the zone corner for the effects of nonlocal charge fluctuations still remains the best option.

IV. RESULTS

A. Correlated metal

Keeping in mind what we expect for weakly correlated metals, we present the results for $U=t^*/2$ at different temperatures in Figs. 2 and 3 for B_{1g} and A_{1g} inelastic x-ray scattering, respectively, as a function of the transferred energy for different momentum transfers throughout the BZ measured by the momentum-space parameter X. Figures 2(a) and 3(a) refer to scattering along the zone diagonal $X=\cos q$ for the zone-diagonal wave vector $\mathbf{q}=(q,q,q,\ldots,q)$, and Figs. 2(b) and 3(b) refer to scattering along the generalized zone edge [here, we have $\mathbf{q}=(q,0,q,0,\ldots,q,0)$ for $1\geqslant X=(1+\cos q)/2\geqslant 0$ and $\mathbf{q}=(\pi,q,\pi,q,\ldots,\pi,q)$ for $0\geqslant X=(-1+\cos q)/2\geqslant -1$]. The curves have been shifted vertically for clarity. The lowest set of curves $X=1$ corresponds to Raman scattering with optical photons.[30]

For the B_{1g} channel (Fig. 2), a well-defined low-energy Fermi-like coherence peak (below $U=0.5t^*$) moves to higher energies and broadens as one moves away from the zone center ($X=1$), as would be expected of Landau damping via particle-hole creation at larger q (Refs. 18 and 31) (recall the Falicov-Kimball model is not a Fermi liquid when $U\neq 0$, but can be viewed as a ''dirty'' Fermi liquid for small

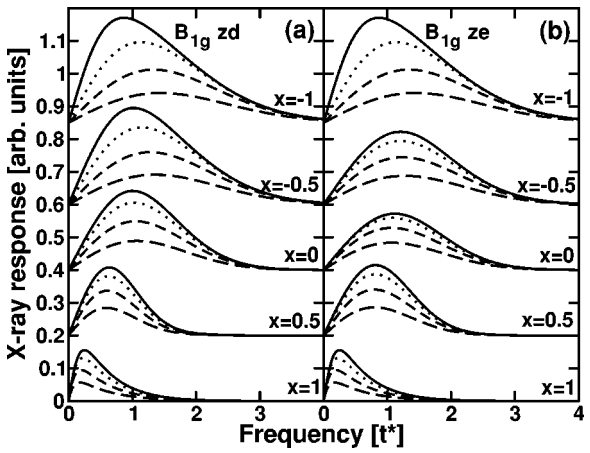

FIG. 2. Inelastic x-ray scattering response for $U=0.5t^*$ in the B_{1g} channel along (a) the BZ diagonal and (b) along the zone edge for the half-filled Falicov-Kimball model on a hypercubic lattice. The solid, dotted, short-dashed, and long-dashed curves correspond to temperatures $T=0.1$, 0.25, 0.5, and 1.0, respectively. The curves have been offset for clarity.

enough U). In addition, the peak sharpens with decreasing temperature as the channels for Landau damping are lost. No particular signature can be seen at the energy transfer of U, since it falls within the line shape of the Fermi-like coherence peak, and thus the role of electronic correlations, while present, are obscured by the larger Landau damping.

In Fig. 4 we plot the position and width of the low-energy peak for the B_{1g} channel for momentum transfers along the BZ diagonal. The peak moves to higher frequencies from $\sim 0.25t^*$ for small momentum transfers $X<1$ and reaches a maximum $\sim t^*$ for momentum transfers slightly greater than $(\pi/2,\pi/2,\ldots)$ before softening as the BZ corner $(\pi,\pi,\ldots)$ is approached. In fact, the peak position is comparable to U for large momentum transfers in all directions. The width of the peak grows continually with increasing $\mathbf{q}$ as more and more phase space is created by which charge excitations may relax. The width initially grows like q^2 for

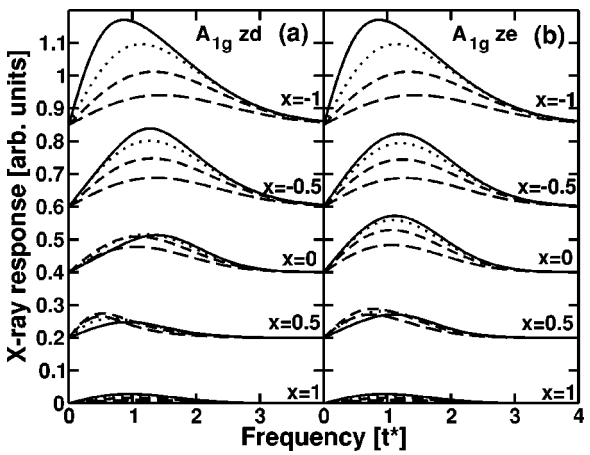

FIG. 3. Inelastic x-ray scattering response $U=0.5t^*$ in the A_{1g} channel along (a) the BZ diagonal and (b) along the zone edge. The solid, dotted, short-dashed, and long-dashed curves correspond to temperatures $T=0.1$, 0.25, 0.5, and 1.0, respectively.

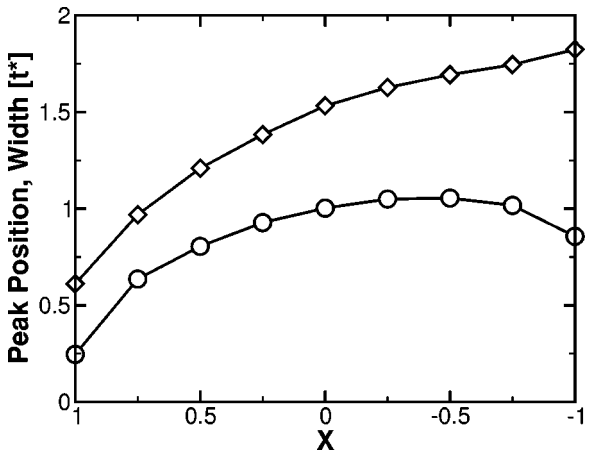

FIG. 4. The position (circles) and the width (diamonds) of the low-energy peak in the B_{1g} channel for momentum transfers along the BZ diagonal for $T=0.1t^*$ as shown in Fig. 2.

momentum transfers away from the BZ center and then slows its growth rate farther from the zone center (recall that $X=\cos q$ so an initial q^2 dependence translates into a linear dependence on X).

An important difference is that the A_{1g} results have no low-energy spectral weight for $\mathbf{q}=0$ as a result of particle-number conservation. In a model with long-range Coulomb interactions, the only excitation would be a high-energy plasmon which is soft for uncharged systems, but is pushed up to higher energies via the Higgs mechanism by the Coulomb interaction. In our short-range model, a mild peak appears on the energy scale of both U and the bandwidth at the zone center (we cannot differentiate which one dominates). The vertex corrections do not completely remove low-energy scattering for any finite value of $\mathbf{q}$, and the low-energy spectral weight grows for increasing $\mathbf{q}$ either along the zone diagonal or the zone edge. For large $\mathbf{q}$, the A_{1g} spectra have a temperature dependence similar to the B_{1g} response, dominated by particle-hole excitations. In fact, the A_{1g} and B_{1g} responses are identical at the $(\pi,\pi,\ldots,\pi)$ point $X=-1$ due to the local approximation. Any variation in the signal at the zone corner in different symmetry channels is due to nonlocal many-body correlations.

For low $\mathbf{q}$ however (such as $X=0.5$), the temperature dependence is nonmonotonic due to a competition between increased vertex corrections, which deplete spectral weight, and decreased particle-hole damping, which aggregates spectral weight into the Fermi-like coherence peak as the temperature is reduced. It is important to note that for an unpolarized (partially polarized) measurement, the x-ray response is a (weighted) superposition of the B_{1g} and A_{1g} spectra. However, the spectra at small $\mathbf{q}$ in a metal would largely have contributions from the B_{1g} channel due to the significant phase-space reduction in the A_{1g} channel.

B. Near critical dynamics

Now we turn to our results for a near critical value of $U=1.5t^*\approx U_c$, where the density of states vanishes at the Fermi level and the system undergoes a metal-insulator tran-

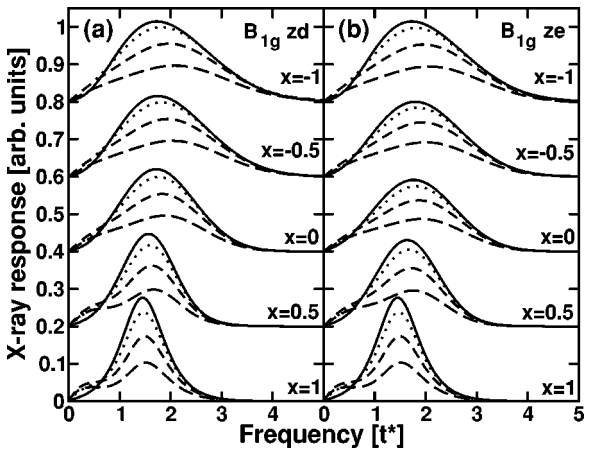

FIG. 5. Inelastic x-ray scattering response $U=1.5t^*$ in the B_{1g} channel along (a) the BZ diagonal and (b) along the zone edge. The solid, dotted, short-dashed, and long-dashed curves correspond to temperatures $T=0.1$, 0.25, 0.5, and 1.0, respectively.

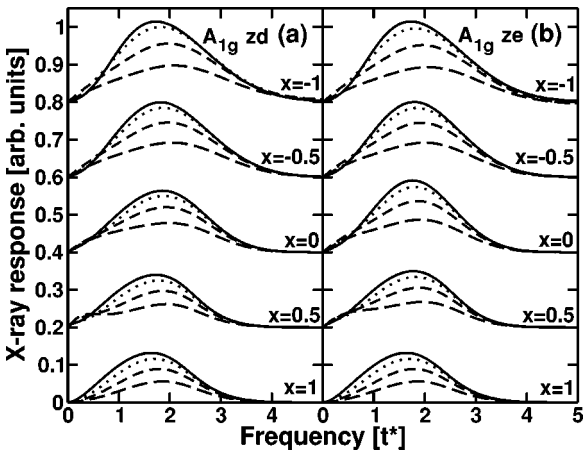

FIG. 6. Inelastic x-ray scattering response $U=1.5t^*$ in the A_{1g} channel along (a) the BZ diagonal and (b) along the zone edge. The solid, dotted, short-dashed, and long-dashed curves correspond to temperatures $T=0.1$, 0.25, 0.5, and 1.0, respectively.

sition (our choice for U lies just on the insulating side of the metal-insulator transition). We plot in Figs. 5 and 6 the results for the B_{1g} and A_{1g} channels, respectively, for the same temperature ranges as in the previous plots. The effect of electronic correlations is clearly visible. For both the B_{1g} and the A_{1g} spectra, two peaks become discernable at small $\mathbf{q}$: the low-energy peak (similar to the one observed for smaller values of U) and a nondispersive high-energy peak (at an energy of roughly U corresponding to transitions between the lower and the upper Hubbard band). Indeed, the results at large $\mathbf{q}$ are more similar to the small U results, since the Landau damping pushes the low-frequency peak into the high-frequency peak and further smears both peaks. Again, the low-energy peak is removed near the zone center for the A_{1g} channel, but in this case the charge-transfer peak (at a frequency near U) remains.

It is important to note that even though the system is near critical, the low-energy spectral weight is visible, particularly in the B_{1g} channel. We now focus on the spectral weight in this region as a function of temperature, shown in Fig. 7. In this low-frequency region, one can clearly see for the B_{1g} channel that the low-energy spectral weight increases with increasing temperature throughout the BZ. This is most clearly seen at $\mathbf{q}=0$. For the A_{1g} channel, the same behavior is masked by the role of vertex corrections which reduce the spectral weight for momentum transfers near the BZ center. Nevertheless, the growth of intensity with increasing temperature is clearly seen in both channels. The growth is particularly clear at low-frequency transfers, and for increasing transfers the effect vanishes and crosses over at larger frequencies to a region where the spectral weight depletes as temperature is increased. The point separating these regions occurs at a crude isosbestic point near $\sim 0.5t^*$, where the spectra are roughly independent of temperature. The isosbestic point becomes less well defined for momentum transfers away from the zone center, and therefore it is most clearly observable in Raman measurements in the B_{1g} channel. As the temperature is increased further, the isosbestic behavior disappears.

C. Insulator

Turning to the insulating phase, our results for $U=2t^*$ for the B_{1g} and A_{1g} channel are shown in Figs. 8 and 9, respectively. Clearly, two features can be resolved in both the B_{1g} and A_{1g} channel: a small, dispersive low-energy peak for frequencies $\sim t^*$ and a large, dispersionless charge-transfer peak $\sim U$ well separated from the low-energy peak. Here, we see more clearly the development of the transfer of spectral weight from low frequencies to higher frequencies as temperature is lowered, with a more clearly defined isosbestic point separating the low- and high-energy transfers, as shown in Fig. 10.

The low-energy depletion of spectral weight and concomitant increase of spectral weight at high energies above the isosbestic point (as T is reduced to zero) was recently discussed in Ref. 14 for $U=4t^*$ (which lies deep on the insulating side of the transition) where the isosbestic point is more clearly observed. The low-energy feature in the insulating phase is determined by thermally generated double

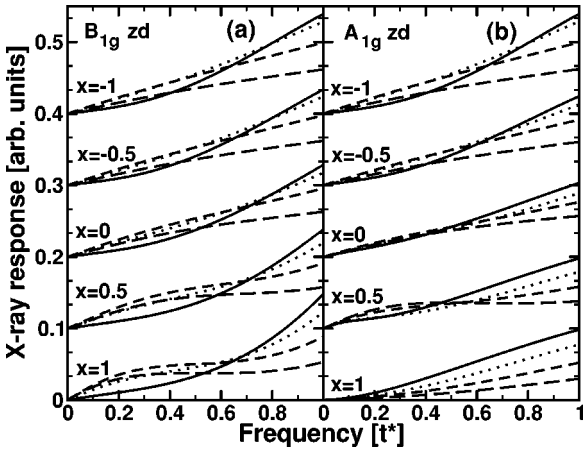

FIG. 7. Detail of the low-energy inelastic x-ray scattering response $U=1.5t^*$ along the zone diagonal for (a) the B_{1g} channel and (b) the A_{1g} channel for the temperatures shown in Figs. 5 and 6.

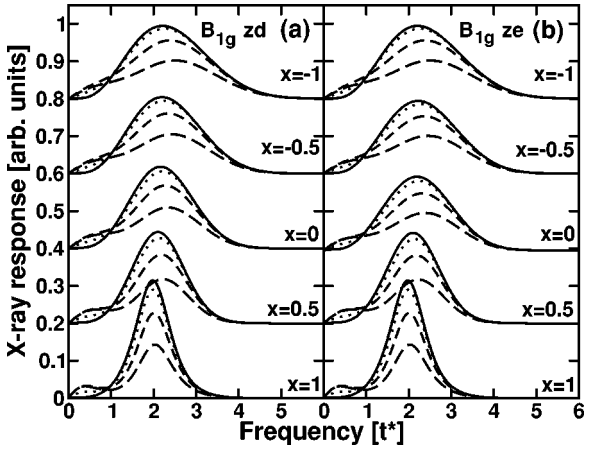

FIG. 8. Inelastic x-ray scattering response $U=2t^*$ in the B_{1g} channel along (a) the BZ diagonal and (b) along the zone edge. The solid, dotted, short-dashed and long-dashed curves correspond to temperatures $T=0.1$, 0.25, 0.5, and 1.0, respectively.

occupancies which become unpopulated at lower temperature. The high-energy peak reflects the energy scale for excitations across the Mott gap and is relatively dispersionless due to the local nature of the correlations. In contrast, the low-energy feature is a consequence of thermally generated double occupancies which open a low-energy band (up to energies $\sim t^*$) able to scatter x rays. The low-energy peak disperses due to Landau damping by the thermally generated excitations, created in greater numbers at larger **q**. These excitations are frozen out for decreasing temperature, and the low-energy intensity disappears. Only scattering across the Mott gap remains at an energy transfer of U. The charge-transfer peak for all **q** broadens for increasing temperature while the low-energy peak gains intensity from zero as temperature is increased, particularly in the B_{1g} channel. As a consequence, both B_{1g} and A_{1g} possess a nondispersive isosbestic point—a frequency at which the spectra are temperature independent—around $\nu\sim U/2$. This result agrees with

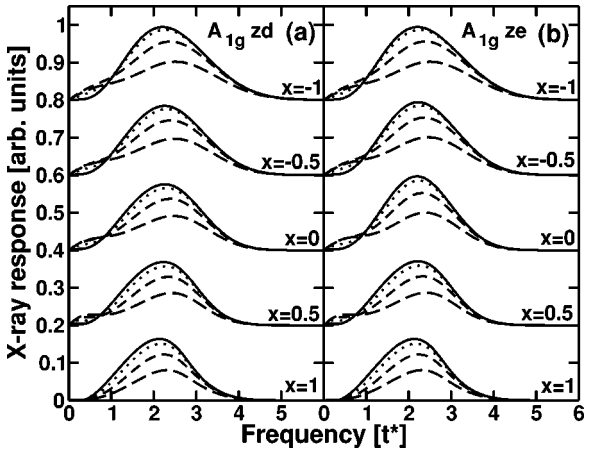

FIG. 9. Inelastic x-ray scattering response $U=2t^*$ in the A_{1g} channel along (a) the BZ diagonal and (b) along the zone edge. The solid, dotted, short-dashed, and long-dashed curves correspond to temperatures $T=0.1$, 0.25, 0.5, and 1.0, respectively.

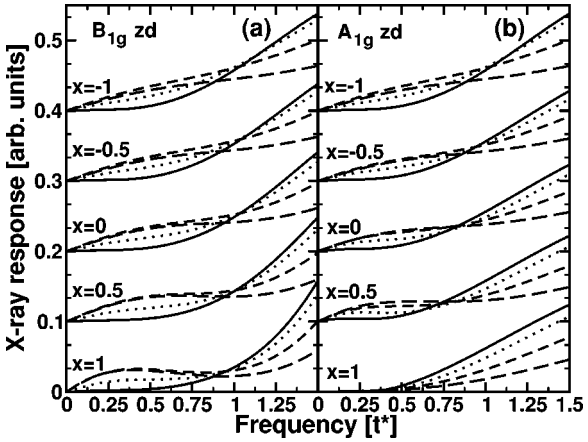

FIG. 10. Detail of the low-energy inelastic x-ray scattering response $U=2t^*$ along the zone diagonal for (a) the B_{1g} channel and (b) the A_{1g} channel for the temperatures shown in Figs. 8 and 9.

our previous results for $U=4$ in which the two peaks are further separated and the isosbestic point is more clearly observed.

We note that even in the insulating case there is no spectral weight at small energy transfers for the A_{1g} channel. Thus we note that regardless of the strength of the correlations, the Raman response ($\mathbf{q}=0$) and the inelastic x-ray response at small **q** should be dominated by the B_{1g} response. This can be an important diagnostic tool for investigating the nature of charge dynamics in different regions of the BZ due to the projection of the B_{1g} scattering amplitude form factors compared to A_{1g}.

V. SUMMARY AND DISCUSSION

In summary, we have constructed a formally exact theory for nonresonant x-ray scattering in a system which can be tuned across a quantum metal-insulator transition. We focused on the polarization and momentum-transfer dependence of the resulting spectra as a way of discerning the role of electron correlations. In particular, the way in which the spectral weight is transferred over different frequency regions as a function of temperature can shed light on the strength of the electronic correlations, and the momentum dependence of the observed spectra can be used to determine ''hot regions'' on the FS. In general, the temperature and polarization dependence of the spectrum would assist in an interpretation of observed peaks in the x-ray spectrum of correlated insulators for example.

In addition, we have pointed out a number of features which reflect the nature of the electronic correlations. One important finding concerns the polarization dependence of the results for momentum transfers at the BZ corner $(\pi,\pi,\ldots,\pi)$. In a theory in which the correlations are purely local, we find that the response function should be identical at this point for both A_{1g} and B_{1g} scattering geometries and that any difference can be attributed to the importance of nonlocal correlations (indeed, they are identical for $-1\leqslant X\leqslant 0$ along the generalized zone boundary). In addition, we have pointed out that for low **q** the full response is

dominated by the B_{1g} channel which projects out particle-hole excitations. Thus in this limit, the excitations can be directly probed and tracked as a function of temperature.

There is currently limited experimental data concerning the polarization and/or temperature dependence of the observed spectra in either correlated metals or insulators and thus many of our predictions remain open to experimental verification. At this stage, current experiments have focused on collective excitations such as the plasmon[3] or orbiton[11] or excitations across a Mott gap in correlated insulators.[5–7,10] Our theory would predict several effects which could serve as a fingerprint of the role of electronic correlations in both correlated metals and insulators by a systematic study of the dependence on temperature and polarization orientations. In particular, one could use x-ray scattering to elucidate electron dynamics near and through a quantum critical metal-insulator transition.

Our theory does not address the role of resonant scattering and the connection to multiband systems. To capture resonance effects, detailed information is needed about the energy separation of the various bands as well as the matrix elements which couple the valence and conduction bands via light scattering. For a Mott insulator this would include resonant transitions between the upper and lower Hubbard bands as well as between excitons. Recently, this has been addressed via exact diagonalization studies[16] and a spin-polaron approach,[17] and its formulation for the Falicov-Kimball model is presently under investigation by us. A more realistic theory for resonant inelastic x-ray scattering should also include resonant transitions in which the deep core hole (created by the incident x-ray) decays via Auger processes and must also include the strong perturbing effect of the core hole on any intermediate states (such as band states or collective modes of the system such as plasmons or magnons) accessible to scattering transitions.[13]

We have also chosen to focus on the paramagnetic metal to paramagnetic-insulator transition. The Falicov-Kimball model, however, possesses phases containing charge order and phase separation. It would be extremely useful to examine the excitations in the ordered phases via light scattering in this model. More generally, dynamical mean-field theory can be used to address the excitations in the ordered phase of this model as well as the Hubbard model.

We conclude with a discussion on the applicability of our results for the limit of large dimensions to finite-dimensional systems. One important consequence of lower dimensions would be that the self-energy and irreducible vertex function will not be strictly local and the momentum dependence may crucially alter not only the formalism but also the spectral evolution of the response as correlations are changed via doping. Particularly, the spectra might show dispersive features which are much more complex than the ones we observed in these calculations. We again note that the inelastic x-ray spectra for momentum transfers at the BZ corner would be very useful to quantify the importance of these nonlocal correlations. One should note, however, that the ''roughness'' of the Fermi surface actually simplifies as the dimensionality is lowered, so the infinite-*d* results already include many complex geometrical effects of the infinite-dimensional hypercubic Fermi surface.

ACKNOWLEDGMENTS

We would like to thank Y.-J. Kim, J. P. Hill, M. V. Klein, and M. van Veenendaal for valuable discussions. J.K.F. acknowledges support from the NSF under Grants Nos. DMR-9973225 and DMR-0210717. T.P.D. acknowledges the support by NSERC and PREA.

[1] For a review, see A. Kotani and S. Shin, Rev. Mod. Phys. **73**, 203 (2001).

[2] A. Shukla, M. Calandra, M. D'Astuto, M. Lazzeri, F. Mauri, C. Bellin, M. Krisch, J. Karpinski, S.M. Kazakov, J. Jun, D. Daghero, and K. Parlinski, Phys. Rev. Lett. **90**, 095506 (2003); B. Ruffle, M. Foret, E. Courtens, R. Vacher, and G. Monaco, *ibid.* **90**, 095502 (2003); M.E. Manley, G.H. Lander, H. Sinn, A. Alatas, W.L. Hults, R.J. McQueeney, J.L. Smith, and J. Willit, Phys. Rev. B **67**, 052302 (2003); T. Scopigno, A. Filipponi, M. Krisch, G. Monaco, G. Ruocco, and F. Sette, Phys. Rev. Lett. **89**, 255506 (2002); S. Raymond, J.P. Rueff, M. D'Astuto, D. Braithwaite, M. Krisch, and J. Flouquet Phys. Rev. B **66**, 220301 (2002); H. Requardt, J.E. Lorenzo, P. Monceau, R. Currat, and M. Krisch, *ibid.* **66**, 214303 (2002); M. d'Astuto, P.K. Mang, P. Giura, A. Shukla, P. Ghigna, A. Mirone, M. Braden, M. Greven, M. Krisch, and F. Sette, Phys. Rev. Lett. **88**, 167002 (2002).

[3] C.A. Burns, P. Giura, A. Said, A. Shukla, G. Vankó, M. Tuel-Benckendorf, E.D. Isaacs, and P.M. Platzman, Phys. Rev. Lett. **89**, 236404 (2002).

[4] A. Cunsolo, G. Monaco, M. Nardone, G. Pratesi, and R. Verbeni, Phys. Rev. B **67**, 024507 (2003).

[5] J.D. Denlinger, J.A. Clack, J.W. Allen, G.-H. Gweon, D.M. Poirier, C.G. Olson, J.L. Sarrao, A.D. Bianchi, and Z. Fisk, Phys. Rev. Lett. **89**, 157601 (2002); L. Journel, J.-M. Mariot, J.-P. Rueff, C.F. Hague, G. Krill, M. Nakazawa, A. Kotani, A. Rogalev, F. Wilhelm, J.-P. Kappler, and G. Schmerber, Phys. Rev. B **66**, 045106 (2002); C. Dallera, M. Grioni, A. Shukla, G. Vankó, J.L. Sarrao, J.P. Rueff, and D.L. Cox, Phys. Rev. Lett. **88**, 196403 (2002).

[6] P. Abbamonte, C.A. Burns, E.D. Issacs, P.M. Platzman, L.L. Miller, S.W. Cheong, and M.V. Klein, Phys. Rev. Lett. **83**, 860 (1999); Y.K. Kim, J.P. Hill, C.A. Burns, S. Wakimoto, R.J. Birgeneasu, D. Casa, T. Gog, and C.T. Venkataramon, *ibid.* **89**, 177003 (2002).

[7] M.Z. Hasan, E.D. Isaacs, Z.-X. Shen, L.L. Miller, K. Tsutsui, T. Tohyama, and S. Maekawa, Science **288**, 1811 (2000); M.Z. Hasan, E.D. Isaacs, Z.-X. Shen, and L.L. Miller, Physica C **364-365**, 618 (2001).

[8] G.P. Zhang, T.A. Callcott, G.T. Woods, L. Lin, B. Sales, D. Mandrus, and J. He, Phys. Rev. Lett. **88**, 077401 (2002).

[9] J.P. Hill, C.-C. Kao, W.A.L. Calieibe, M. Matsubara, A. Kotani, J.L. Peng, and R.L. Greene, Phys. Rev. Lett. **80**, 4967 (1998); K.

Hämäläinen, J.P. Hill, S. Huotari, C.-C. Kao, L.E. Berman, A. Kotani, T. Idé, J.L. Peng, and R.L. Greene, Phys. Rev. B **61**, 1836 (2000).
[10] M.Z. Hasan, P.A. Montano, E.D. Isaacs, Z.-X. Shen, H. Eisaki, S.K. Sinha, Z. Islam, N. Motoyama, and S. Uchida, Phys. Rev. Lett. **88**, 177403 (2002); (private communication).
[11] T. Inami, T. Fukuda, J. Mizuki, S. Ishihara, H. Kondo, H. Nakao, T. Matsumura, K. Hirota, Y. Murakami, S. Maekawa, and Y. Endoh, Phys. Rev. B **67**, 045108 (2003)
[12] Y.-J. Kim and J. P. Hill (private communication).
[13] P.M. Platzman and E.D. Isaacs, Phys. Rev. B **57**, 11 107 (1998).
[14] T.P. Devereaux, G.E.D. McCormack, and J.K. Freericks, Phys. Rev. Lett. **90**, 067402 (2003).
[15] J.K. Freericks, T.P. Devereaux, R. Bulla, and Th. Pruschke, Phys. Rev. B **67**, 155102 (2003).
[16] K. Tsutsui, T. Tohyama, and S. Maekawa, Phys. Rev. B **61**, 7180 (2000); H. Kondo, S. Ishihara, and S. Maekawa, *ibid.* **64**, 014414 (2001); **64**, 179904(E) (2001); K. Okada and A. Kotani, *ibid.* **65**, 144530 (2002); K. Tsutsui, T. Tohyama, and S. Maekawa, cond-mat/0303242 (unpublished).
[17] P. Wróbel and R. Eder, Phys. Rev. B **66**, 035111 (2002).
[18] P. Nozieres and D. Pines, *Theory of Quantum Liquids*, Perseus Books (Cambridge, University Press, Cambridge, 1966).
[19] T.P. Devereaux, Phys. Rev. B **45**, 12965 (1992).
[20] A. Virostek and J. Ruvalds, Phys. Rev. B **45**, 347 (1992).
[21] T.P. Devereaux and A.P. Kampf, Phys. Rev. B **59**, 6411 (1999).
[22] L.M. Falicov and J.C. Kimball, Phys. Rev. Lett. **22**, 997 (1969).
[23] W. Metzner and D. Vollhardt, Phys. Rev. Lett. **62**, 324 (1989).
[24] P.G.J. van Dongen and D. Vollhardt, Phys. Rev. Lett. **65**, 1663 (1990); P.G.J. van Dongen, Phys. Rev. B **45**, 2267 (1992); P.G.J. van Dongen and C. Leinung, Ann. Phys. (Leipzig) **6**, 45 (1997).
[25] U. Brandt and C. Mielsch, Z. Phys. B: Condens. Matter **75**, 365 (1989); V. Zlatić, J.K. Freericks, R. Lemański, and G. Czycholl, Philos. Mag. B **81**, 1443 (2001); J. K. Freericks and V. Zlatić, Rev. Mod. Phys. (to be published).
[26] M. Jarrell, Phys. Rev. Lett. **69**, 168 (1992).
[27] E. Müller-Hartmann, Z. Phys. B: Condens. Matter **74**, 507 (1989); **76**, 211 (1989); Int. J. Mod. Phys. B **3**, 2169 (1989).
[28] A. Khurana, Phys. Rev. Lett. **64**, 1990 (1990).
[29] A.M. Shvaika, Physica C **341-348**, 177 (2000); J.K. Freericks and P. Miller, Phys. Rev. B **62**, 10 022 (2000); A.M. Shvaika, J. Phys. Stud. **5**, 349 (2002).
[30] J.K. Freericks and T.P. Devereaux, Condens. Matter Phys. **4**, 149 (2001); Phys. Rev. B **64**, 125110 (2001); J.K. Freericks, T.P. Devereaux, and R. Bulla, *ibid.* **64**, 233114 (2001).
[31] L.D. Landau, J. Phys. (USSR) **10**, 25 (1946).